

Article

Charge Carrier Formation following Energy Gap Law in Photo-Activated Organic Materials for Efficient Solar Cells

Aniket Rana ^{1,2,3,*}, Nikita Vashistha ^{3,4,†}, Amit Kumar ^{3,5,†}, Mahesh Kumar ^{3,6,*} and Rajiv K. Singh ^{3,5,*}

¹ Department of Chemistry, Imperial College London, London W12 0BZ, UK

² Centre for Processable Electronics, Imperial College London, London SW7 2AZ, UK

³ Academy of Scientific and Innovative Research (AcSIR), CSIR-NPL Campus, New Delhi 110012, India; nikita.vashistha@uni-jena.de (N.V.); kumaramitiitg004@gmail.com (A.K.)

⁴ Institute of Physical Chemistry, Friedrich Schiller University Jena, Helmholtzweg, 4, 07743 Jena, Germany

⁵ CSIR—National Physical Laboratory, Dr. K.S. Krishnan Marg, New Delhi 110012, India

⁶ Innovation and Management Directorate Council of Scientific and Industrial Research, Anusandhan Bhawan, New Delhi 110001, India

* Correspondence: aniket.rana@imperial.ac.uk (A.R.); mkumar@csir.res.in (M.K.); rajivsingh@nplindia.org (R.K.S.)

† These authors contributed equally to this work.

Abstract: The charge carrier formation and transport in the pristine polymers as well as in the polymer–fullerene blend is still a hot topic of discussion for the scientific community. In the present work, the carrier generation in some prominent organic molecules has been studied through ultrafast transient absorption spectroscopy. The identification of the exciton and polaron lifetimes of these polymers has led to device performance-related understanding. In the Energy Gap Law, the slope of the linear fit gradient (γ) of lifetimes vs. bandgap are subjected to the geometrical rearrangements experienced by the polymers during the non-radiative decay from the excited state to the ground state. The value of gradient (γ) for excitons and polarons is found to be -1.1 eV^{-1} and 1.14 eV^{-1} , respectively. It suggests that the exciton decay to the ground state is likely to involve a high distortion in polymer equilibrium geometry. This observation supports the basis of Stokes shift found in the conjugated polymers due to the high disorder. It provides the possible reasons for the substantial variation in the exciton lifetime. As the bandgap becomes larger, exciton decay rate tends to reduce due to the weak attraction between the holes in the HUMO and electron in the LUMO. The precise inverse action is observed for the polymer–fullerene blend, as the decay of polaron tends to increase as the bandgap of polymer increases.

Keywords: organic solar cell; carrier dynamics; energy gap law



Citation: Rana, A.; Vashistha, N.; Kumar, A.; Kumar, M.; Singh, R.K. Charge Carrier Formation following Energy Gap Law in Photo-Activated Organic Materials for Efficient Solar Cells. *Energies* **2024**, *17*, 2114. <https://doi.org/10.3390/en17092114>

Academic Editor: Philippe Leclère

Received: 6 September 2023

Revised: 10 October 2023

Accepted: 6 December 2023

Published: 28 April 2024



Copyright: © 2024 by the authors. Licensee MDPI, Basel, Switzerland. This article is an open access article distributed under the terms and conditions of the Creative Commons Attribution (CC BY) license (<https://creativecommons.org/licenses/by/4.0/>).

1. Introduction

The π -conjugated polymer-based organic solar cells have attracted the thoughtful attention of scientists and engineers in recent years due to their electronic property, flexibility, ease of processing, low cost, and provision of an effective alternative in comparison to the inorganic solar cells. [1]. In spite of the significant advancement in the development of organic solar cell technology, the complexities of charge carrier generation and evolution in pristine as well as in the donor–acceptor (D–A) blend are still under the emphasis of fundamental research directed towards the development of noble donor–acceptor materials [2]. The π -conjugated polymer backbone chain contains a series of overlapping σ orbitals arranged through sp^2 hybridization. In such an arrangement, π -electrons remain unbounded, thereby producing a conjugated chain of delocalized π -electrons [3]. The high anisotropic quasi-one-dimensional (1D) electronic structure is found in these organic semiconductors which are fundamentally different from the inorganic semiconductors [4], thereby having different photoexcitation processes. The mixture of two organic semiconductor solution blends termed as donor (D) and acceptor (A), respectively, develops the

photoactive layer with nanoscale domains in the organic solar cells [5]. The realization of these nano domains is currently the key factor in generating highly efficient organic solar cells. Despite important developments in the understanding of how the device works, the details of charge carrier generation and evolution of a D–A blend for the organic solar cell are still the emphasis of fundamental research. The process of charge carrier generation [6] in the polymer–fullerene blend is usually described through the following steps: (1) the absorption of photons with appropriate energy in the polymer domain to generate excitons; (2) the diffusion of excitons towards the polymer–fullerene interface through Brownian motion; (3) the transfer of electron from donor (polymer) to acceptor (fullerene), which gives birth to the polarons; however, the substantial Coulomb attraction and wave function overlap between the electron polaron in the acceptor and hole polaron in the donor domain results in the creation of charge transfer (CT) state; and (4) the dissociation of these CT state and free carrier transport towards the respective electrodes. The discussion over the existence and identification of a CT state is still a hot topic among researchers. Initially, there was a simple concept regarding the generation of free carriers in the D–A blend system, i.e., the diffusion of a generated exciton in a donor towards the D–A interface followed by an ultrafast dissociation of exciton without any intermediate state. However, after the evolution of many spectroscopic techniques, the CT state was confirmed [7]. The generation of excitons and polarons after the photoexcitation are the fundamental events in organic solar cells. However, in particular, there are not any explicit approaches available to optimize the lifetime of these fundamental charge species. The present work aims to provide an analysis of exciton and polaron generation as well as their lifetime in the pristine and D–A blend, respectively, for some significant different donor–acceptor molecules. The lifetime is tested with the Energy Gap Law for all polymers [8,9].

2. Experimental Methods

Ultrafast Transient Absorption Spectroscopy

Thin layers of donor and donor–acceptor were applied onto quartz glass plates using a spin-coating technique to conduct UV-Vis and ultrafast transient absorption spectroscopy investigations. Prior to this, individual solutions of donor and donor–acceptor were prepared, each with a concentration of 5 mg/mL in a nitrogen-filled glovebox so that 50% transparency could be maintained for ultrafast transient absorption spectroscopy measurement. DTS(FBTTh₂)₂ and PC[70]BM were mixed in a 6:4 wt% ratio, PCE10 and PC[70]BM in a 1:1.5 wt% ratio, PCDTBT and PC[70]BM in a 1:4 wt% ratio, and PBDTT-DPP and PC[70]BM in a 1:2 wt% ratio. The ultrafast transient absorption spectroscopy experimental setup employed a Ti:Sapphire femtosecond laser to both pump and probe the samples. To examine carrier relaxation dynamics, an ultrafast transient absorption spectrometer (Helios by Ultrafast Systems) was combined with an amplified Ti:Sapphire laser (Legend by Coherent) and an oscillator (Micra by Coherent). The output from the Micra oscillator, which produced laser pulses at 800 nm wavelength, 80 MHz repetition rate, and 45 fs pulse width, was directed towards a regenerative amplifier. The output was then routed through stretcher/compressor gratings. The resultant laser pulse had a width of 45 fs, operated at an 800 nm wavelength, had a 1 kHz repetition rate, and had an average energy output of 4 mJ. To achieve the required wavelengths, 50% of this output was fed into an optical parametric amplifier (TOPAS by Light Conversion). From this output, 25% was utilized to create a white light spectrum through a Sapphire disk, serving as the probe pulse source. The remaining 25% was employed for generating higher harmonic frequencies. The optical parametric amplifier (OPA) generated a femtosecond pulse within the range of 190 to 2600 nm, with a pulse width of 70 fs, used to pump the sample. For the purpose of obtaining the difference spectra (ΔA) signal, the pump signal was reduced to 500 Hz through a chopper. Both beams (pump and WL probe) were made to overlap over the sample to capture absorption spectra in the ‘with’ and ‘without’ pump conditions. The transient behavior of a sample was obtained by delaying the probe wrt to pump. A highly stable 450 nm pump beam ($P_{avg} = 0.5$ mW) was utilized to stimulate

carriers within the samples. By monitoring changes in the optical properties, such as reflectivity, or in the transmission of the sample over varying time delays between the pump and probe pulses and from visible to NIR probe wavelength, valuable insights into the relaxation behavior of electronic states within the sample were garnered. This methodology enabled the measurement of electronic excitation lifetimes with a resolution down to the femtosecond time scale. Absorption and steady-state fluorescence spectroscopy experiments were conducted using a UV-vis spectrophotometer (SHIMADZU UV-1800 UV-VisSpectrophotometer, 190 nm to 1100 nm) and a Fluorolog spectrofluorometer (Jobin Yvon-Horiba, model 3-11), respectively. DTS(FBTTh₂)₂ and PC[70]BM were mixed in a 6:4 wt% ratio, PCE10 and PC[70]BM in a 1:1.5 wt% ratio, and PCDTBT and PC[70]BM in a 1:4 wt% ratio in chlorobenzene, while PBDTT-DPP and PC[70]BM were in a 1:2 wt% ratio in dichlorobenzene.

3. Result and Discussion

3.1. Organic Donor and Acceptor Molecules for Solar Cells

Here some organic molecules are introduced that are commonly employed as donor-acceptor materials in organic solar cells. Polymers, oligomers, and small molecules with conjugated backbones are being used as electron donor materials in organic solar cell devices. Despite the differences in the categories of these compounds, for photo activity, the requirement and properties are relatively similar. The photo absorber layers are preferred to grow as a micro-crystalline structural phase. The microcrystalline structure increases exciton diffusion length and charge carrier mobility [10,11] because the grain boundaries are the main limitation for these factors.

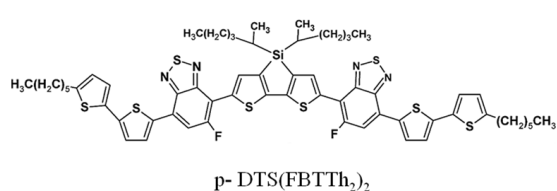
Mainly two approaches are followed to estimate the morphological and energetic properties: First, the functional group application, which is an electron donating or withdrawing group. These groups are defined at the specific location of the orbitals and therefore describe the type of molecules. More specifically, these particular groups define the π -system in the molecule, either being a strong donor or acceptor. The second approach is the difference in the size and arrangement of the aromatic system that contributes to the π -system. The size of the molecules mainly affects the highest occupied molecular orbital (HOMO) and lowest unoccupied molecular orbital (LUMO) gap. The three dimensional arrangement of the molecule can change the morphology of the molecular film. The side groups in the molecule are free to rotate, which can be activated by the temperature, and which reduces the possibility to crystallize molecular film. There are two ways that functional groups can affect the energy levels in any molecule. First, there can be an inductive effect, which acts on the σ -bond between the two different atoms having different electronegativity. The atoms or the functional group with a high electronegativity will have a high electron withdrawing property and will also have a high positive partial charge remaining in the core of the molecule [12]. The second is called the mesomeric effect, which acts on conjugated π bonds.

Figure 1 shows the chemical structure of organic molecules frequently used for solar cell device fabrication. In recent times, a number of small donor molecules with promising electronic and optical properties have been reported for organic solar cells [13,14]. The small molecule offers a well-defined structure and has no molecular weight dependence compared to the polymeric counterpart, leading to improved purity as well as limitations in batch-to-batch variation inconsistency. They also exhibit an organized structure leading to high charge carrier mobility. Figure 1a shows the 7,7'-(4,4-bis(2-ethylhexyl)-4H-silolo[3,2-b:4,5-b']dithiophene-2,6-diyl)bis(6-fluoro-4-(5'-hexyl-[2,2'-bithiophen]-5-yl)benzo[c][1,2,5]thiadiazol) (p-DTS(FBTTh₂)₂) molecular structure. In this figure, “p” denotes the fluorine atoms oriented proximally to the inner fragment. The incorporation of 5-fluorobenzo[c][1,2,5]thiadiazole (FBT) as an acceptor unit is a key feature of this molecule. Bazan et al. have given the five step synthesis scheme for p-DTS(FBTTh₂)₂ in detail [15]. The success of this kind of molecular architecture is largely dependent on the inclusion of a [1,2,5]-thiadiazolo-[3,4-c]-pyridine heterocycle (also known as pyridyl[2,1,3]thiadiazole, abbreviated as PT), which is an electron-deficient unit [16]. The architecture of such a

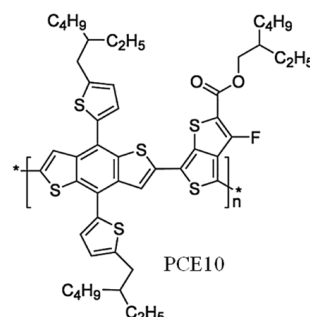
molecule consists of an acceptor–donor–acceptor (ADA) core flanked with end-capping units. The two acceptor units are used to increase the electron affinity across the conjugated backbone confirming deep HOMO level whereas the end-capping unit is utilized to extend π -conjugation and tailor self-assembly properties. The coupling of PT to the available conjugated block also provides chromospheres with the required light harvesting properties [17]. The association of PT provides another advantage in that pyridyl nitrogen gives asymmetry in such a way that near quantifiable site-selective cross-coupling is achieved through the 4,7-dibromo-[1,2,5] thiadiazole [3,4-c]pyridine precursor [18–20] and this reactivity is appropriate to the synthesis of p-DTS(FBTTh₂)₂. A solar cell efficiency of 6.7% based on the combination of p-DTS(FBTTh₂)₂ and PC70BM has been achieved [21]. The HOMO and LUMO level of p-DTS(FBTTh₂)₂ has subsequently been found to be –5.1 and –3.3 eV and has been depicted in Figure 2. The design of low bandgap polymers began with the introduction of D–A alternating copolymers [22]. P3HT is a homopolymer that uses a single moiety as a repeating unit whereas low bandgap polymers incorporate an alternating backbone between one electron rich moiety (donor) and one deficient moiety (acceptor). The HOMO and LUMO energy levels of such types of polymers are determined by the HOMO energy level of the donor moiety and the LUMO energy levels from the acceptor moiety [23]. Therefore, energy level tuning can be achieved by modifying the functional group for the donor–acceptor unit [24]. The Stille polycondensation method is highly modest for the synthesis of such low bandgap polymers due to the wide variety of available functional groups. The benzo[1,2-b:4,5-b']dithiophene (BDT) unit proved to be an important electron-rich component for high-performing organic solar cells. The PTB series polymers uses a BDT and thieno[3,2-b]thiophene (TT) unit, developed by Yu and coworkers through the Stille polycondensation method with a Pd(PPh₃)₄ catalyst mixed with toluene/DMF solvent at 120 °C to enhance the organic solar cell performance [25,26]. The high molecular weight can be achieved for the PTB series polymers due to their excellent solubility, which permits them to stay in the solution until the large polymer chain growth. In 2010, PTB7 was developed and the combination with PC70BM resulted in a 7.4% efficient solar cell being achieved using the conventional structure [27]. Yu and his team also synthesized fluorinated derivatives of PTB polymers to understand the effect of fluorine substitution on the performance of PTB polymers [28]. They found that fluorination on the TT unit improves the polarization of polymers which assists the charge carrier separation more effectively. The synthesis of PTB polymers with the enhanced 2D structure of the π -bonding system was achieved by attaching aromatic side chains to the BDT unit, which also enhances the coplanarity of the polymer backbone. This kind of organization favors the π -stacking and charge transport properties in the polymers, resulting in several kinds of polymers with alternate Fluorinated TT and BDT-Th units [29]. Cao and his team demonstrated a 9.94% efficient solar cell from a PTB7-Th/PC71BM blend [30]. PTB7-Th is also well known as PBDTTT-EFT and PCE10 (Poly[4,8-bis(5-(2-ethylhexyl)thiophen-2-yl)benzo[1,2-b;4,5-b']dithiophene-2,6-diyl-alt-(4-(2-ethylhexyl)-3-fluorothieno[3,4-b]thiophene)-2-carboxylate-2-6-diyl]), which is shown in Figure 1b. The HOMO and LUMO level of PCE10 has subsequently been found to be –5.2 and –3.6 eV and is depicted in Figure 2. In Figure 1c, another efficient polymer named Poly[N-9'-heptadecanyl-2,7-carbazole-alt-5,5-(4',7'-di-2-thienyl-2',1',3'-benzothiadiazole)], Poly[[9-(1-octynonyl)-9H-carbazole-2,7-diyl]-2,5-thiophenediyl-2,1,3-benzothiadiazole-4,7-diyl-2, thiophenediyl] (PCDTBT) is shown, which is usually synthesized by the Suzuki polycondensation of the carbazole boronic acid and thietylbenzothiadiazole derivative in a biphasic solvent system employing toluene and an aqueous base [31,32]. The required monomer concentration in such kinds of polymerizations is comparatively high (~0.2 M), and it is also occasionally problematic to fully dissolve all reaction components. The replacement of the hexyl derivative (C₆H₁₃) permitted the flow synthesis of the PCDTBT analog PCDHTBT. The HOMO and LUMO level of PCDTBT was subsequently found to be –5.5 and –3.6 eV and is depicted in Figure 2. In addition, Yang et al. [33] combined the 2D-BDT unit in the DPP-based polymers to achieve high performance low bandgap Poly{2,6'-4,8-di(5-ethylhexylthienyl)benzo[1,2-b;3,4-b]dithiophene-

alt-5,5'-dibutyloctyl-3,6-bis(5-thiophen-2-yl)pyrrolo[3,4-c]pyrrole-1,4-dione (PBDTT-DPP) polymers. The chemical structure of PBDTT-DPP is shown in Figure 1d. The PBDTT-DPP polymers play a vital role in achieving highly efficient semi-transparent tandem organic solar cells [33] with efficiency >9%. The HOMO and LUMO levels of PBDTT-DPP were subsequently found to be -5.3 and -3.6 eV and are depicted in Figure 2.

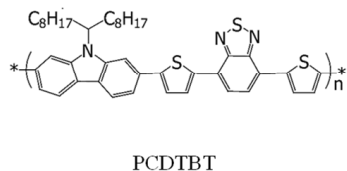
(a)



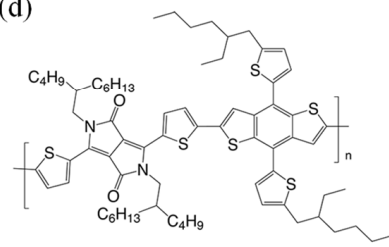
(b)



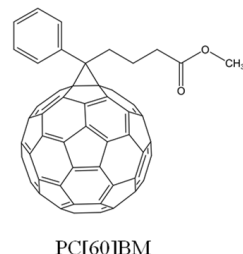
(c)



(d)



(e)



(f)

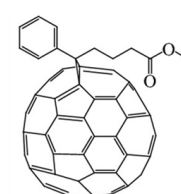


Figure 1. Chemical molecular structure and abbreviations of organic donor and acceptor materials used for organic solar cells: (a) DTS(FBTTh₂)₂; (b) PCE10; (c) PCDTBT; (d) PBDTT-DPP; (e) PC[60]BM; and (f) PC[70]BM.

The above-mentioned conjugated polymers and small molecules are excellent electron donor materials, and they also exhibit potential properties of electron acceptors, but only a few electron acceptor materials have a high potential for organic solar cell devices. Fullerene and its derivative are proven to be the most efficacious electron acceptor materials. Fullerene C₆₀ has a symmetrical structure and demonstrates excellent electron mobility. It is well known that one C₆₀ molecule can accept four electrons, hence C₆₀ is an efficient acceptor. Sariciftci et al. discovered an ultrafast electron-accepting capability from donor to C₆₀ molecule [34].

C₆₀ can be dissolved in chlorobenzene (CB) or 1,2-Dichlorobenzene (DCB) seamlessly, but it shows limited solubility in other organic solvents. To improve the solubility and also to reduce the degree of phase separation in the donor–acceptor blend, [6,6]-phenyl-C₆₁-butyric acid methyl ester (PC[60]BM) was applied to an inorganic solar cell. The chemical structure of PC[60]BM is shown in Figure 1e. In the past few decades, PC[60]BM and its derivative C₇₀ (PC[70]BM) have been used predominantly as acceptor materials in organic solar cells. PC[60]BM, and PC[70]BM, comprises strong absorption in the visible range, therefore, it has attracted more attention recently. However, the tedious synthesis and purification method of PC[70]BM makes it more expensive, which limits its application. The molecular structure of PC[70]BM is shown in Figure 1f. The HOMO and LUMO levels

of PC[60]BM and PC[70]BM are depicted in Figure 2. They exhibit similar HOMO levels but have differences in the LUMO level on an order of 0.5 eV. The absorption spectra for PC[60]BM and PC[70]BM are depicted in Figure 3e. The optical properties, assessed using UV-Vis absorption spectroscopy, of the above-mentioned donor polymers, including their blend with a PCBM acceptor, are shown in Figure 3. The solutions were prepared in chlorobenzene and spin-casted on a quartz glass plate. The p-DTS(FBTTh₂)₂ and PC[70]BM are mixed in a 6:4 wt% ratio. p-DTS(FBTTh₂)₂ exhibits wide low-energy transition and good overlap with the solar spectrum, with λ_{max} 650 nm as depicted in Figure 3a. The absorption spectrum shows $\pi-\pi^*$ vibronic transition peaks at ~380 nm and ~720 nm, which is typically an indication of the ordered film [35].

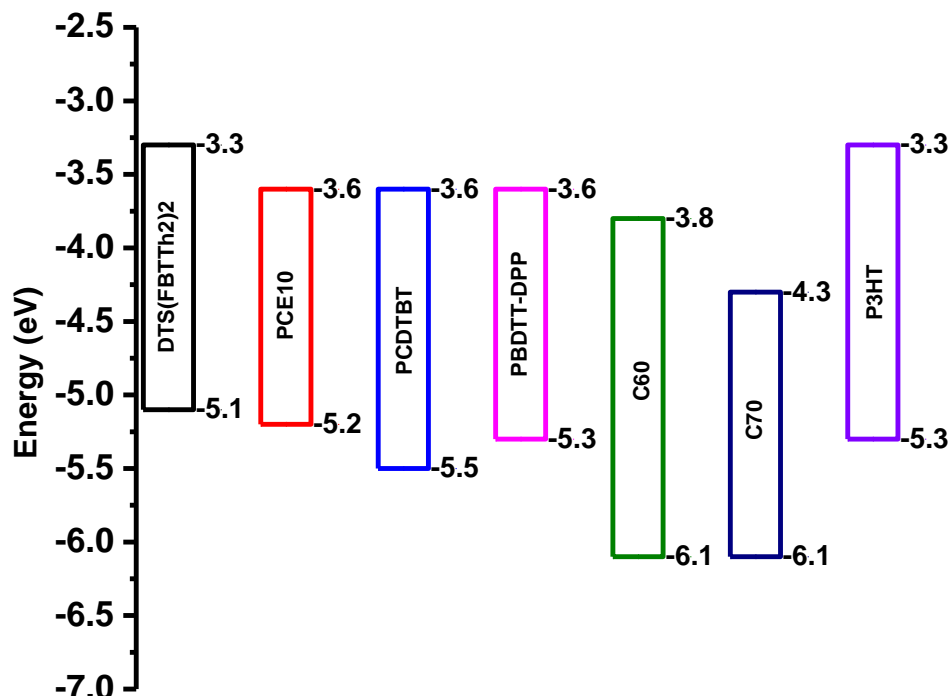


Figure 2. HOMO and LUMO energy levels of different donor–acceptor molecules viz. DTS(FBTTh₂)₂, PCE10, PCDTBT, PBDTT-DPP, PC[60]BM, PC[70]BM, and P3HT.

The absorption spectra of p-DTS(FBTTh₂)₂ with PC[70]BM shows ~20 nm blue shift in the λ_{max} as compared to the neat film due to the deaggregation of the p-DTS(FBTTh₂)₂ molecule within the blend. This phenomenon arises as PC[70]BM disrupts the intermolecular interaction and molecular packing of p-DTS(FBTTh₂)₂ [36]. The wide absorption spectra for PCE10 and PCE10:PC[70]BM are shown in Figure 3b. The blend ratio for PCE10 and PC[70]BM is 1:1.5 wt%. It has a $\pi-\pi^*$ transition peak at ~630 nm and ~710 nm. When mixed with PC[70]BM, a small red shift in the transition peak is observed due to the aggregation effect. The pure PCDTBT absorption spectra shown in Figure 3c has two prominent peaks at 400 nm and 550 nm due to the acceptor–donor copolymers feature. The 400 nm peak is attributed to the $\pi-\pi^*$ transition to the 550 nm peak, which is attributed to the interchain charge transfer [37]. When mixed with PC[70]BM in a 1:4 wt% ratio, the absorption peak at 550 nm shows broadening. In Figure 3d, the absorption spectrum for PBDTT-DPP and PBDTT-DPP:PC[70]BM (1:2 wt%) are shown. Pure PBDTT-DPP film shows broad absorption range from 500 nm to 850 nm, which makes it highly suitable for tandem solar cells. It has $\pi-\pi^*$ transition peaks at ~700 nm and ~730 nm. In the case of DTS(FBTTh₂)₂:PC[70]BM, it is evident that the donor–acceptor ratio is 6:4 wt%, signifying a higher proportion of the donor component when compared to the acceptor. This led to a decrease in the absorption of pure p-DTS(FBTTh₂)₂ in comparison to the absorption observed in the DTS(FBTTh₂)₂:PC[70]BM blend. When we contrast this donor–acceptor ratio with other systems, we can observe a lower quantity of the donor relative to the

acceptor in these systems, resulting in reduced absorption in the blend as compared to the pure film.

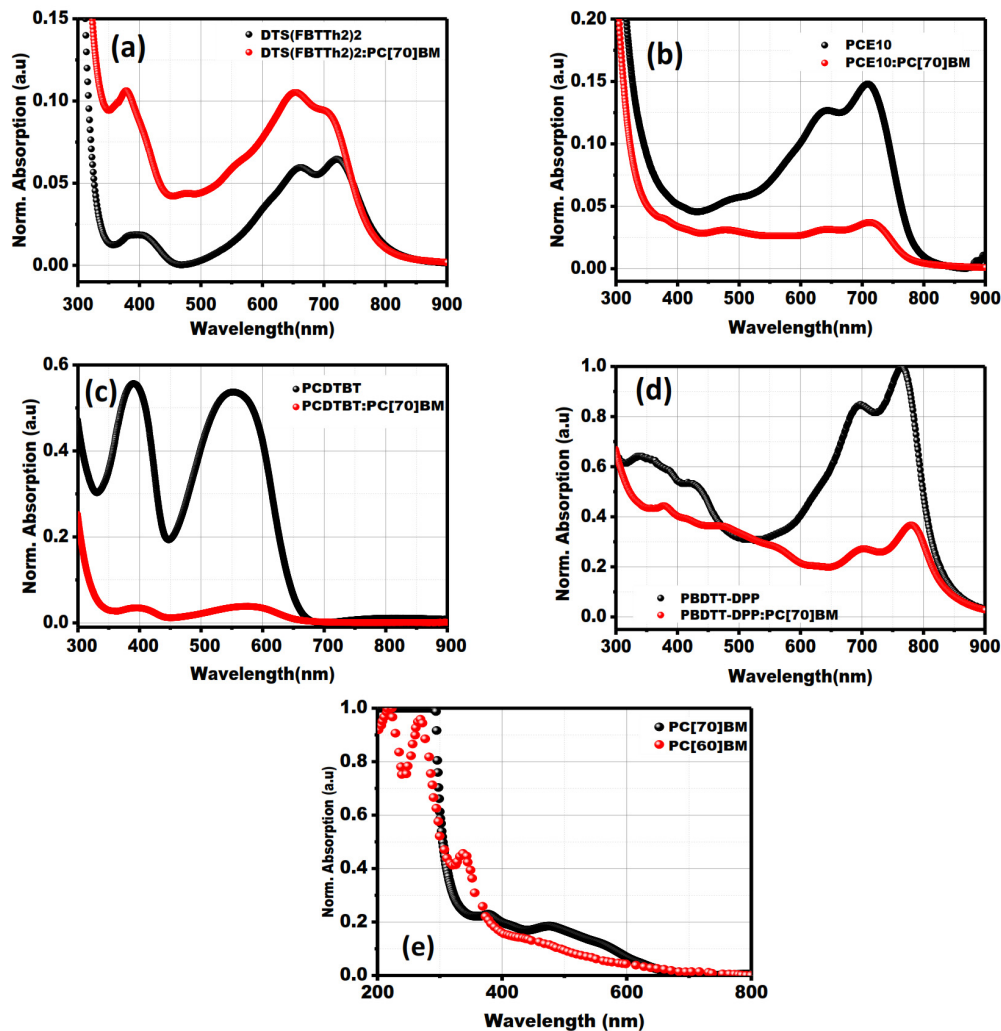


Figure 3. Absorption spectrum of donor and donor acceptor blend. Red and black lines (a–d) represent the donor only and donor–acceptor blend, respectively. (a) DTS(FBTTh₂)₂ and DTS(FBTTh₂)₂:PC[70]BM; (b) PCE10 and PCE10:PC[70]BM; (c) PCDTBT and PCDTBT:PC[70]BM; (d) PBDTT-DPP and PBDTT-DPP:PC[70]BM; and (e) PC[60]BM and PC[70]BM.

To access the evidence of exciton dissociation efficiency, a photoluminescence (PL) measurement was performed in the pristine and blend forms of all above-mentioned polymers as depicted in Figure 4. The excitation wavelength was guided through the absorption spectrum (Figure 3) for each type of polymer. Figure 4a shows the PL spectrum of DTS(FBTTh₂)₂ and DTS(FBTTh₂)₂:PC[70]BM. With the excitation wavelength of 600 nm, the emission spectrum is located in the range of 700 nm to 850 nm.

In the blend film, complete quenching indicates efficient exciton generation. Similar strong quenching is also observed in the PCE10:PC[70]BM blend as shown in Figure 4b when excited with a 500 nm light source. However, broad emission is observed in the case of pure PCE10 ranging from 700 nm to 850 nm. The PL spectra for PCDTBT and PCDTBT:PC[70]BM is shown in Figure 4d. The emission spectrum for pure PCDTBT is observed from 620 nm to 800 nm, when excited with a 500 nm source. The efficient PL quenching indicates the fast electron transfer from the LUMO of PCDTBT to the LUMO of PC[70]BM. In Figure 4d, the PL spectrum for PBDTT-DPP and PBDTT-DPP:PC[70]BM is presented for the excitation wavelength of 550 nm. In this case, quenching is not very

efficient hence the exciton formation is not as good as compared to the other polymers, therefore, this polymer is not usually used in single donor structure organic solar cells. Hence it is more suitable for tandem structure solar cells in which a wide range of solar spectrum absorption needs to be covered.

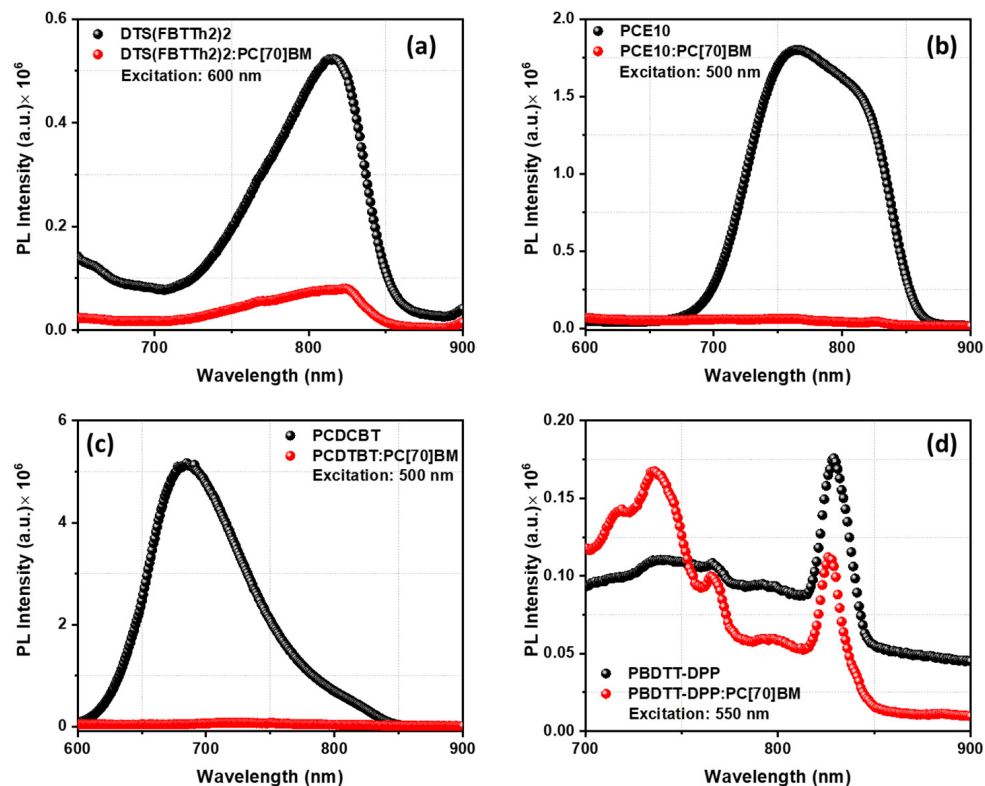


Figure 4. Photoluminescence spectrum of donor and donor acceptor blend. Red and black lines represent the donor only and donor acceptor blend respectively. (a) DTS(FBTTh₂)₂ and DTS(FBTTh₂)₂:PC[70]BM (b) PCE10 and PCE10:PC[70]BM (c) PCDCBT and PCDTBT:PC[70]BM (d) PBDTT-DPP and PBDTT-DPP:PC[70]BM.

3.2. Ultrafast Transient Photophysics of Organic Donor and Acceptor Molecules

3.2.1. DTS(FBTTh₂)₂ and DTS(FBTTh₂)₂:PC[70]BM

Here, a detailed discussion is presented regarding charge carrier generation in the above-mentioned donor–acceptor molecules. The ultrafast transient absorption spectroscopy (UTAS) technique is applied to present the basic principle of carrier dynamics in polymeric films. Figure 5a–f corresponds to the UTAS experiment results taken for DTS(FBTTh₂)₂ and DTS(FBTTh₂)₂:PC[70]BM. The decay-associated spectra is recorded for DTS(FBTTh₂)₂ from 0 s to 6 ns with 480 nm pump excitation for visible and NIR. The ground state bleaching (GSB) occurs immediately after the excitation ranging from 550 nm.

The maxima of GSB signal occurs at ~950 fs with a peak at 714 nm and has a decay lifetime of 46 ps. In the near-infrared region (1000–1400 nm), UTAS spectra show a positive absorption called photoinduced absorption (PIA). The PIA peak at 1195 nm is assigned to the singlet excited state for pristine DTS(FBTTh₂)₂, depicted in Figure 5a [38]. The best fitting for the carrier lifetime at different wavelengths has been calculated with the multi-exponential equation as given below.

$$\Delta A(\lambda, t) = A_1(\lambda) \exp\left(-\frac{t}{\tau_1}\right) + A_2(\lambda) \exp\left(-\frac{t}{\tau_2}\right) + A_3(\lambda) \exp\left(-\frac{t}{\tau_3}\right) \quad (1)$$

τ_1 is fast and assigned to non-radiative decay and A_3 and τ_3 have been ignored as an offset of measurement. Therefore, the characteristics lifetime for charge species is assigned

through τ_2 only. The lifetime of a singlet exciton is found to be 31.7 ps, as given in Table S1. The other wavelengths such as 469 nm and 595 nm provide information regarding the excitation of different vibronic states in the material.

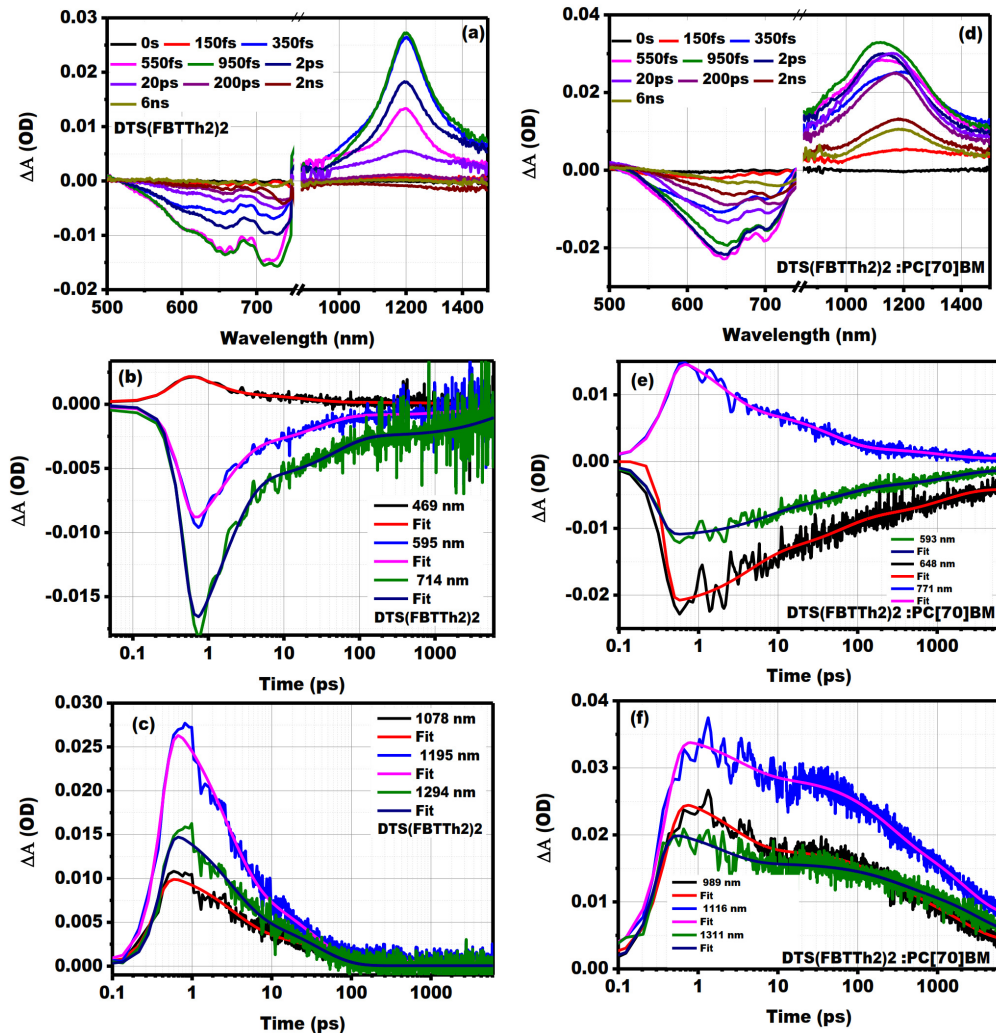


Figure 5. The relative differential absorption spectra (ΔA (OD)) with respect to the wavelength over Vis-NIR at various probe delay times and decay kinetics. (a) ΔA (OD) for DTS(FBTTh₂)₂; (b) decay kinetics for DTS(FBTTh₂)₂ in visible spectrum; (c) decay kinetics for DTS(FBTTh₂)₂ in NIR spectrum; (d) ΔA (OD) for DTS(FBTTh₂)₂:PC[70]BM; (e) decay kinetics for DTS(FBTTh₂)₂:PC[70]BM in visible spectrum; and (f) decay kinetics for DTS(FBTTh₂)₂:PC[70]BM in NIR spectrum.

The carrier decay profile for pristine DTS(FBTTh₂)₂ at different prominent wavelengths is shown in Figure 5b,c and their calculated lifetimes have been given in Table S1. The UTAS spectra for DTS(FBTTh₂)₂:PC[70]BM has been given in Figure 5d. The excitation wavelength for the blend has been kept similar to the pristine film. The excitation wavelength was chosen around the absorption minimum for DTS(FBTTh₂)₂ and near to the absorption maxima of PC[70]BM so that the contribution of PC[70]BM could be examined. The GSB signal shows a blue shift in the blend compared to the pristine film due to the interaction of PC[70]BM with the backbone of the DTS(FBTTh₂)₂ chain by affecting the crystallinity nature of the film. In the blend, a higher and more intense GSB signal is achieved at 550 fs, which is before the pristine film, and which confirms the electron transfer from DTS(FBTTh₂)₂ to PC[70]BM. After that, these electrons transferred into the PC[70]BM form the polaron in the blend. The broad PIA signal in the near-NIR region starts to occur within 150 ps, which confirms the ultrafast carrier fetching capability of PC[70]BM [39] that is also

confirmed in the PL spectrum. The lifetime of polarons at the 1116 nm wavelength is found to be 2.2 ns, which implies long-lived charge transfer (CT) states in these polymers.

3.2.2. PCE10 and PCE10:PC[70]BM

Another class of highly efficient polymer is PCE10, belonging to the PTB family. The charge carrier generation in PCE10 and PCE10:PC[70]BM has been studied using a UTAS experiment as given in Figure 6. Figure 6a represents the transient spectra from visible to NIR for pristine PCE10 film and Figure 6b,c shows decay kinetic spectra at different wavelengths. In pristine PCE10, the film shows GSB signal maxima at ~708 nm immediately after the excitation from the 480 nm pump wavelength. The maximum bleach recovery signal is achieved at ~550 fs, and within 2 ns, an 80% recovery of GSB is observed. The lifetime at different prominent wavelengths has been given in Table S2. Here, different wavelengths correspond to the vibronic ($\pi-\pi^*$) transition. In the NIR region, a broad PIA peak is observed for singlet excitons with the highest peak observed at 350 fs. Within 20 ps, the PIA signal completely disappeared, which refers to the complete annihilation of excitons. The PIA signal is much broader than that of DTS(FBTTh₂)₂, hence, larger number of excitons are available. When PC[70]BM is mixed with PCE10 as an acceptor, the changes in the GSB and PIA signal are observed as shown in Figure 6d. The slower change in the GSB signal is perceived in the case of the PCE10:PC[70]BM film compared to the PCE10 film. The broad PIA signal pertains until 2 ns in the case of the blend film. There are two prominent PIA peaks that exist in the PCE10:PC[70]BM film. The first peak, at ~877 nm, corresponds to the localized polaron pair and the other peak, at ~1072 nm, is consequently attributed to delocalized polaron pairs. The kinetics of charge species in PCE10:PC[70]BM at the corresponding wavelength are given in Figure 6e,f. The lifetime of the localized polaron pair at ~877 nm was found to be 884 ps, and the lifetime of the delocalized polaron pair at ~1072 nm was found to be 979 ps. Other kinetics at 970 nm give the highest polaron life time of up to 1 ns, which indicates the longer CT states in the PCE10:PC[70]BM film as shown in Table S2. Due to the large CT state or polaron lifetime, a better short circuit current is achieved in such polymers.

3.2.3. PCDTBT and PCDTBT:PC[70]BM

Figure 7 shows the UTAS for PCDTBT and PCDTBT:PC[70]BM over the visible to NIR spectral range. The UTAS for pristine PCDTBT is shown in Figure 7a with the excitation pump wavelength of 420 nm. The GSB signal results in the range of absorption spectrum. In the pristine film, the maxima of the GSB signal is achieved in the range of 550 to 950 ps. The very broad PIA signal occurs from 620 nm to 1400 nm with two different segments.

The first PIA signal ranging from ~620 nm to ~800 nm lies in the range of the photoluminance spectrum which originated from the stimulated emission (SE). Beyond this range, PIA is the signature peak of the associated localized states [40]. Figure 7b,c shows the decay kinetics for the charge carrier species generated in visible and NIR regions. The GSB signal at ~553 nm exhibits an initial fast and nonradiative decay in the range of 2 ps followed by a slower component decay in the range of 1 ns. The decay of the SE signal (~658 nm) is also observed in the range of 1 ns which indicates the long lifetime for higher electronic states. The UTAS obtained for the PCDTBT:PC[70]BM blend has been given in Figure 7d and the corresponding decay kinetics in Figure 7e,f. The blend film shows similar spectral behavior with the difference in the early ground state bleaching (GSB) compared to the pristine film, which indicates the transfer of an electron from the donor to the fullerene. The blend also exhibits a shorter lifetime in the GSB range and longer lifetime in the PIA regime as shown in Table S3. The polaron lifespan in the blend is in the order of 1.5 ns, which infers an enhanced photoconductivity and better charge separation at the interface.

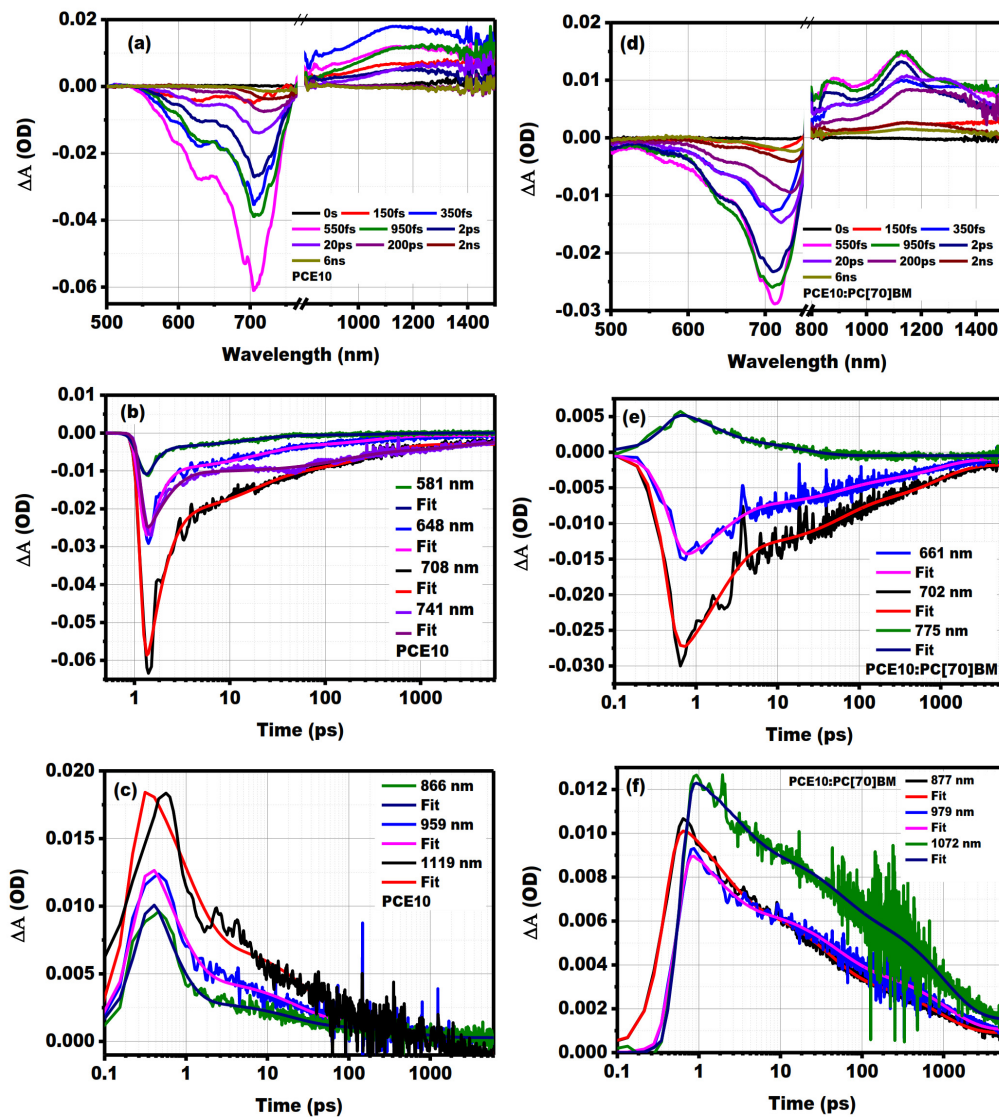


Figure 6. The relative differential absorption spectra ($\Delta A(\text{OD})$) with respect to the wavelength ranging over visible to NIR at various probe delay times and decay kinetics. (a) $\Delta A(\text{OD})$ for PCE10; (b) decay kinetics for PCE10 in visible spectrum; (c) decay kinetics for PCE10 in NIR spectrum; (d) $\Delta A(\text{OD})$ for PCE10:PC[70]BM; (e) decay kinetics for PCE10:PC[70]BM in visible spectrum; and (f) decay kinetics for PCE10:PC[70]BM in NIR spectrum.

3.2.4. PBDTT-DPP and PBDTT-DPP:PC[70]BM

Figure 8 represents the UTAS measurement result for another important organic molecule, i.e., PBDTT-DPP and PBDTT-DPP:PC[70]BM. The PBDTT-DPP is an NIR light-sensitive polymer. It has strong photosensitivity at 600 to 750 nm; therefore, the GSB occurs in this range with a decay time of 28 ps, as given in Table S4. It also exhibits a very broad PIA signature ranging from 850 nm to 1500 nm. Around 550 fs, the maximum GSB peak is observed, similar to the previous organic molecules.

Figure 8b,c shows kinetics at different prominent wavelengths to give the nature of carrier decay in GSB and PIA regions. When mixed with PC[70]BM, it does not show good quenching as shown in the photoluminescence spectra. The PIA shows a very short lifetime in the range of 30 ps. Therefore, it is not suitable for the single donor–acceptor organic solar cell structure. The kinetic is fitted with the three exponential time constants but the third time constant is ignored as offset due to the very small pre-exponential weightage

(A3). Since the discovery of fullerene, it has attracted interest, particularly as an acceptor molecule in organic solar cells.

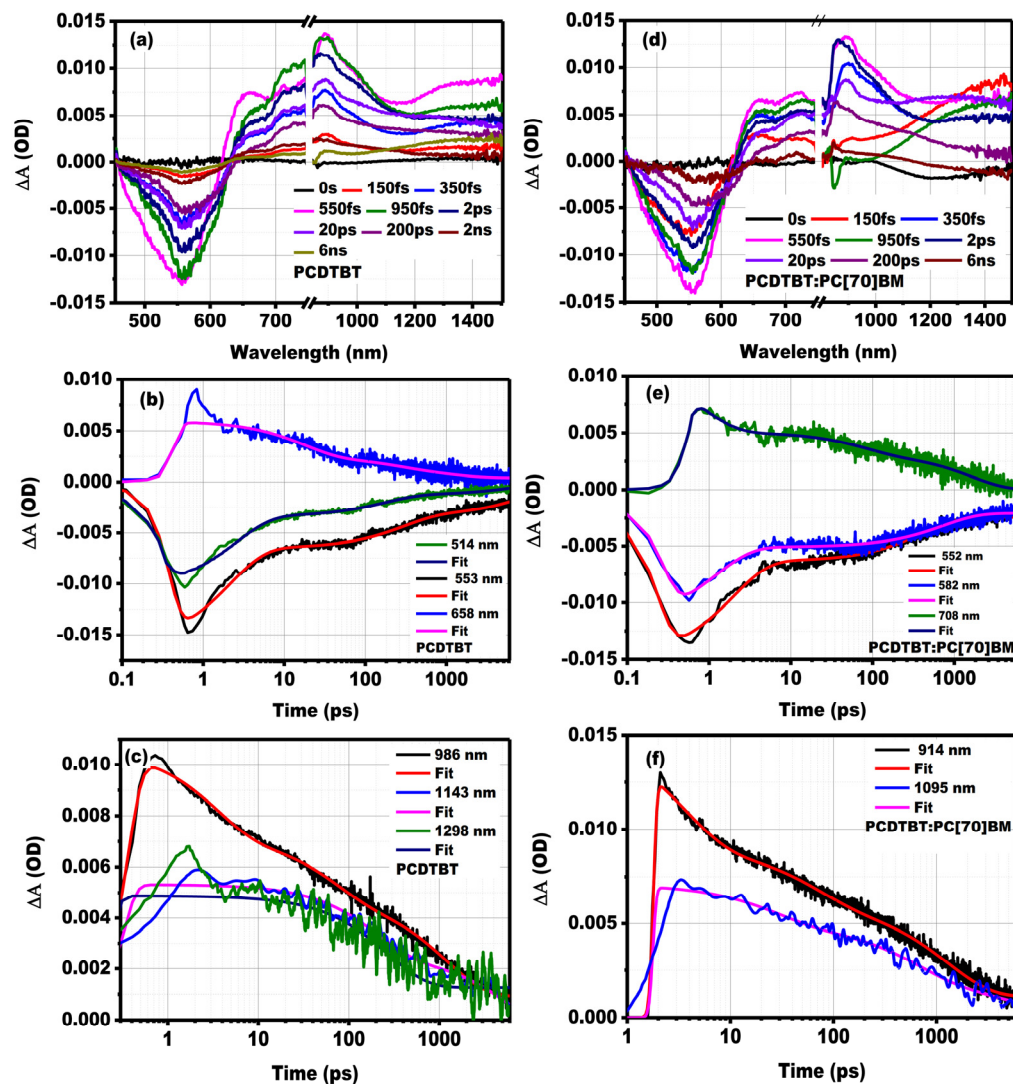


Figure 7. The relative differential absorption spectra ($\Delta A(\text{OD})$) with respect to the wavelength ranging over visible to NIR at various probe delay times and decay kinetics. (a) $\Delta A(\text{OD})$ for PCDTBT; (b) decay kinetics for PCDTBT in visible spectrum; (c) decay kinetics for PCDTBT in NIR spectrum; (d) $\Delta A(\text{OD})$ for PCDTBT:PC[70]BM; (e) decay kinetics for PCDTBT:PC[70]BM in visible spectrum; and (f) decay kinetics for PCDTBT:PC[70]BM in NIR spectrum.

3.2.5. PC[60]BM and PC[70]BM

The soluble fullerene derivative [6,6]-phenyl C₆₀ butyric acid methyl ester (PC[60]BM) and the similar C₇₀ (PC[70]BM) have been ubiquitously used as acceptors. In this section, the photophysical properties of PC[60]BM and PC[70]BM have been discussed with the help of UTAS measurements. Their absorption profiles have already been discussed in Figure 3.

These show strong absorption at 300 nm, with weak absorption above this. In comparison to PC[60]BM, PC[70]BM has better absorption in the visible region up to 600 nm. Therefore, the carrier generated in such a molecule cannot be avoided, which has not been discussed in detail until today. In Figure 9, the UTAS result for PC[60]BM has been given in the visible to NIR region with the pump excitation of 375 nm. The pristine PC[60]BM strikingly shows the PIA feature extended from 500 nm to 1400 nm. The prominent peaks are apparent in the visible region around 492 nm and 725 nm.

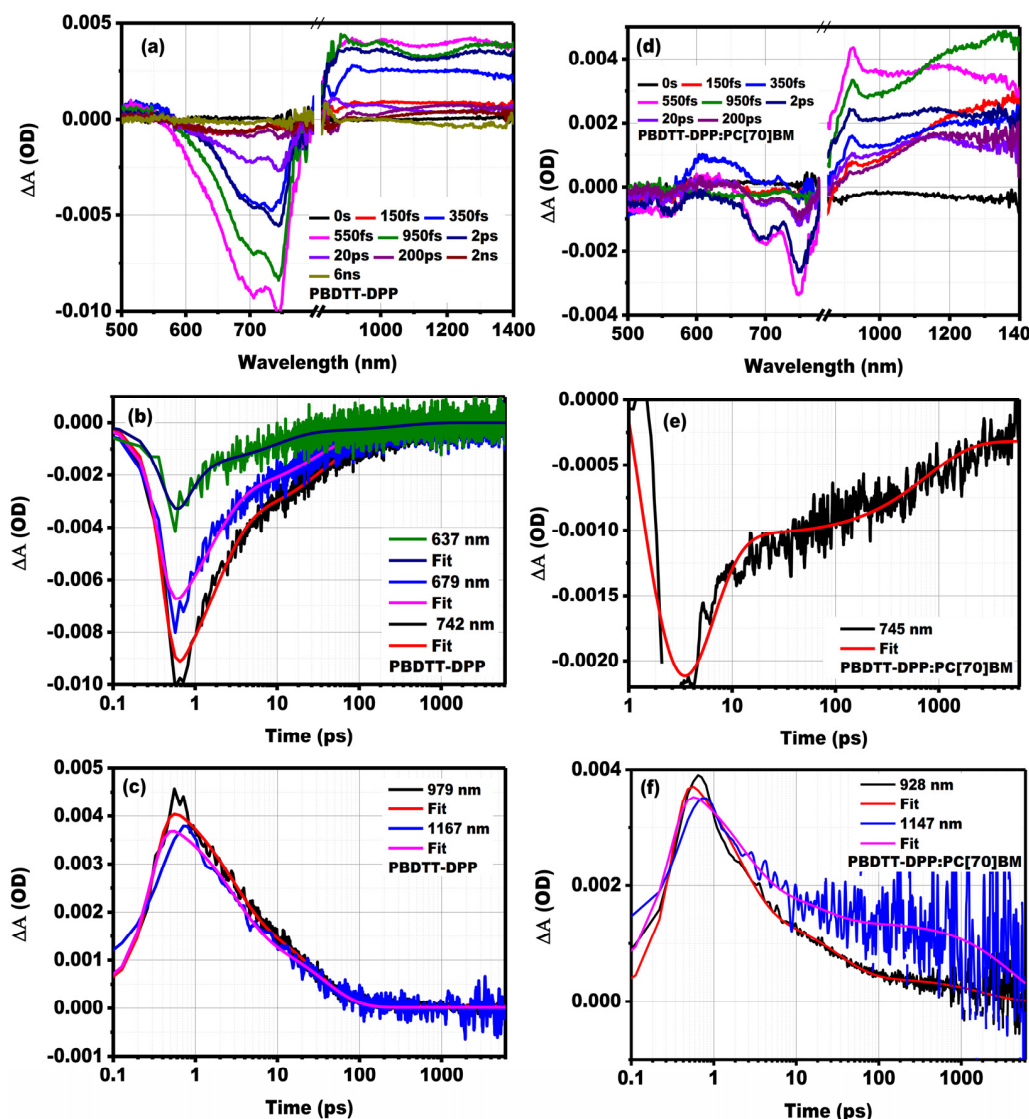


Figure 8. The relative differential absorption spectra ($\Delta A(\text{OD})$) with respect to the wavelength ranging over visible to NIR at various probe delay times and decay kinetics. (a) $\Delta A(\text{OD})$ for PBDTT-DPP; (b) decay kinetics for PBDTT-DPP in visible spectrum; (c) decay kinetics for PBDTT-DPP in NIR spectrum; (d) $\Delta A(\text{OD})$ for PBDTT-DPP:PC[70]BM; (e) decay kinetics for PBDTT-DPP:PC[70]BM in visible spectrum; and (f) decay kinetics for PBDTT-DPP:PC[70]BM in NIR spectrum.

The lifetime of these singlet excitons are in the range of 1 ns as depicted in Table S5. Some studies also show that PC[60]BM mixed with polystyrene (PS) may produce triple excitons through intersystem crossing [41]. The PIA around 500 nm has been assigned to an electroabsorbance signal deriving from the high polarizability of C₆₀ [42]. The PIA in the NIR region in the range of 800 to 1200 nm occurs due to the fullerene anion absorption [43]. These spectral features are the indication of charge generation rather than neutral exciton formation in the PC[60]BM film. The signal around 725 nm has been attributed to the triplet formation in the presence of oxygen as the experiment is performed in the ambient condition [41]. Bernardo et al. have reported that the high dielectric screening in the fullerene nanocrystal produces a delocalized CT state dissociation [44]. The low dielectric constant of PCBM (3.9) increases the spatial separation in the molecule, which reduces the electronic interaction that results in the relatively localized and more strongly bound excitons in the blend film [45]. In Figure 10, the UTAS measurement of PC[70]BM has been given, and the pump wavelength was kept similar to the PC[60]BM. In the PC[70]BM, a much broader PIA is observed in the visible region ranging from 450 to 800 nm due to the better absorption

in the visible region. The maximum decay at 719 nm is observed up to 973 ps. In the NIR region, PC[70]BM exhibits broad absorption, which indicates a better generation of charge carrier in the pristine film compared to the PC[60]BM. In both PCBM molecules, the ability to separate charges may also be related to the dependence of PCBM LUMO level upon aggregation states, with local deviations in the degree of crystallization providing an energetic offset to favor charge separation. The overall comparative representation of UTAS measurement response for pristine polymers and their blend with fullerene is shown in Figure 11a,b. The transient absorption of pristine polymers shows the GSB in different wavelength ranges according to their static absorptions. The DTS(FBTTh₂)₂ and PCE10 have a much broader GSB signature compared to the other polymers containing a larger coverage of visible spectrum.

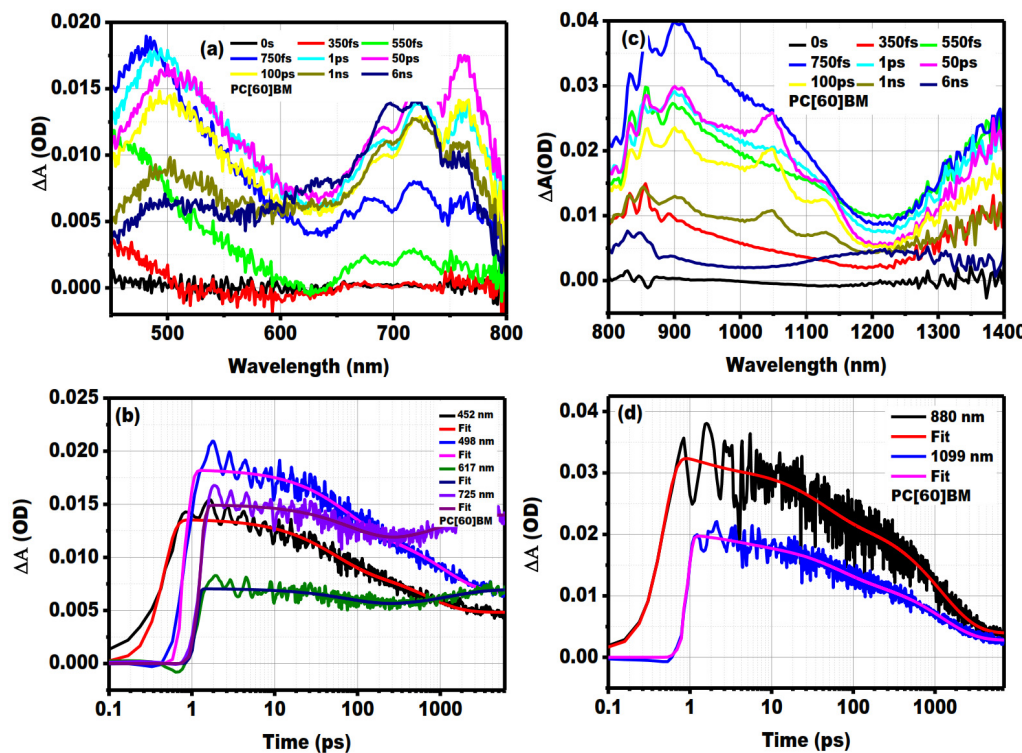


Figure 9. The relative differential absorption spectra ($\Delta A(\text{OD})$) with respect to the wavelength ranging over visible to NIR at various probe delay times and decay kinetics for PC[60]BM. (a) $\Delta A(\text{OD})$ for visible region; (b) decay kinetics in visible region; (c) $\Delta A(\text{OD})$ in NIR region; and (d) decay kinetics in NIR region.

The PIA for pristine polymers also has a different coverage range of spectrum from visible to NIR. With PCDTBT, PIA starts from the visible to NIR region. The calculation of average exciton lifetime has been evaluated from the global fitting of PIA for every polymer. Due to the complex spectral decay, the excitonic lifetime was taken from the three exponential fits. Similarly, the spectral decay of the polymer–fullerene blend is given in Figure 11b. The average lifetime of polarons has been calculated from the global fitting of PIA in the region.

Figure 12 represents the plot of the natural logarithm of the inverse of exciton and polaron lifetimes vs. the optical bandgap of all polymers mentioned earlier as given in Table 1. This allows us to test the Energy Gap Law for polymers. According to the Energy Gap Law, the slope of the linear fit gradient (γ) is subject to the geometrical rearrangements experienced by the polymers during the non-radiative decay from the excited to the ground state. The value of gradient (γ) for excitons and polarons is subsequently found to be -1.1 eV^{-1} and 1.14 eV^{-1} [9]. Thus, it suggests that the exciton decay to the ground state in the above-mentioned photo-activated polymer is likely to involve a high distortion of

polymer equilibrium geometries. This observation supports the basis of the Stokes shift found in the conjugated polymers due to the high disorder.

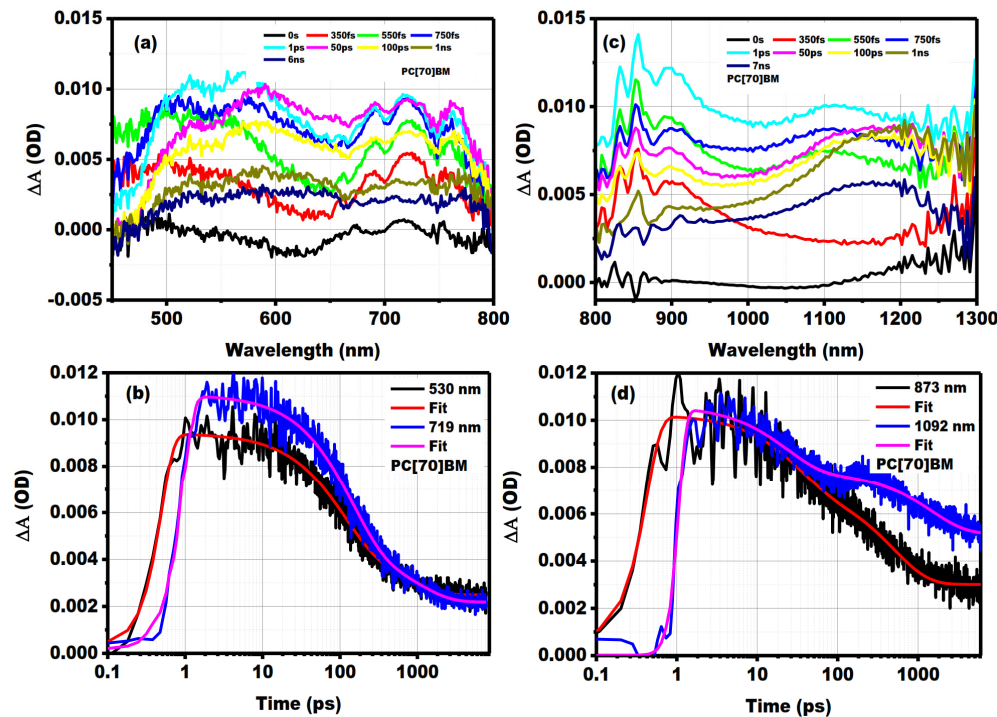


Figure 10. The relative differential absorption spectra ($\Delta A(\text{OD})$) with respect to the wavelength ranging over visible to NIR at various probe delay times and decay kinetics for PC[70]BM. (a) $\Delta A(\text{OD})$ for visible region; (b) decay kinetics in visible region; (c) $\Delta A(\text{OD})$ in NIR region; and (d) decay kinetics in NIR region.

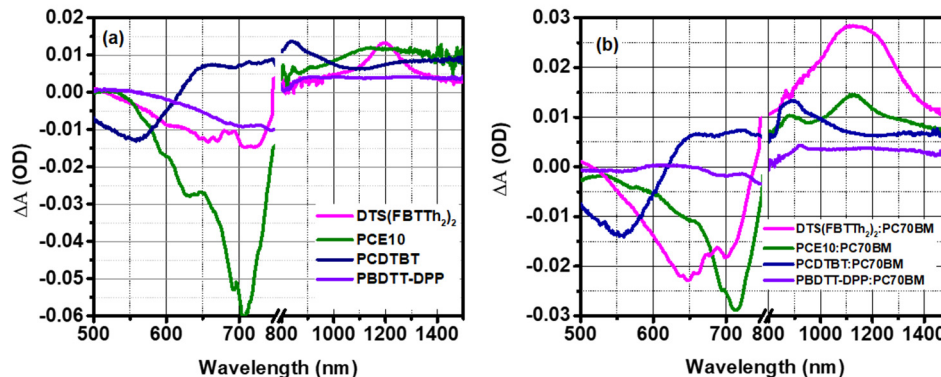


Figure 11. The comparison of differential absorption spectra ($\Delta A(\text{OD})$) for (a) pristine polymers and (b) blend with fullerene at 550 ps.

Table 1. Optical bandgap and exciton polaron lifetime for polymers extracted from the global analysis of UTAS data.

Polymers	E_g (eV)	Exciton (ps)	$k_e = 1/(\tau_{\text{exciton}})$	Polaron (ps)	$k_p = 1/(\tau_{\text{polaron}})$
PCE10	1.6	124	0.008064516	1536	0.000651042
PBDTT-DPP	1.7	266	0.003759398	1890	0.000529101
DTFS(FBTTh ₂) ₂	1.8	95	0.010526316	1452	0.000688705
PCDTBT	1.9	649	0.001540832	1111	0.00090009
P3HT [45]	2.0	187	0.005347594	708	0.001412429
PC[60]BM	2.3	1186	0.00084317	—	—
PC[70]BM	1.8	867	0.001153403	—	—

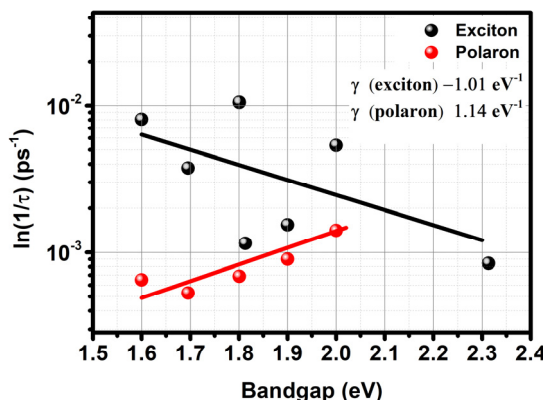


Figure 12. The natural logarithm of the decay rate of the exciton (black sphere) and polaron (red sphere) decay plotted for the above-mentioned polymers calculated from the UTAS. The solid line represents the best fit to the decay rate of exciton and polaron.

4. Conclusions

Here we conclude that as the bandgap becomes larger, the exciton decay rate decreases due to the weaker attraction between the holes in the HUMO and electron in the LUMO that causes substantial variation in the exciton lifetimes. The precise inverse action is observed for the polymer–fullerene blend, the decay of the polaron tends to increase as the bandgap of polymer improves. Therefore, it shows a positive gradient (γ) of an order of 1.14 eV^{-1} . It concludes that in the low bandgap polymers, the conversion of exciton to polaron is high, therefore producing better current and efficiency. Additionally, a similar investigation of non-fullerene acceptor-based systems has the potential to offer more fundamental insights into the effective generation of free charges, even in cases with a low energy offset.

Supplementary Materials: The following supporting information can be downloaded at: <https://www.mdpi.com/article/10.3390/en17092114/s1>, Table S1. The lifetime of excited carriers and associated pre-exponential amplitude for DTS(FBTTh2)2 and DTS(FBTTh2)2:PC[70]BM at different wavelength after multi-exponential fitting. Table S2. The lifetime of excited carriers and associated pre-exponential amplitude for PCE10 and PCE10:PC[70]BM at different wavelength after multi-exponential fitting. Table S3. The lifetime of excited carriers and associated pre-exponential amplitude for PCDTBT and PCDTBT:PC[70]BM at different wavelength after multi-exponential fitting. Table S4. The lifetime of excited carriers and associated pre-exponential amplitude for PBDTT-DPP and PBDTT-DPP:PC[70]BM at different wavelength after multi-exponential fitting. Table S5. The decay kinetics of PC[60]BM at different wavelength according to Figure 9. Table S6. The decay kinetics of PC[70]BM at different wavelength according to Figure 10.

Author Contributions: Conceptualization, A.R.; Methodology, N.V. and M.K.; Validation, A.R.; Writing—original draft, A.R.; Writing—review & editing, N.V. and A.K.; Supervision, M.K. and R.K.S. All authors have read and agreed to the published version of the manuscript.

Funding: This research received no external funding.

Data Availability Statement: Data is contained within the article.

Acknowledgments: The authors are thankful to the Director, National Physical Laboratory, Dr. K.S. Krishnan Road, New Delhi, for his kind support. The authors gratefully recognize the financial support from the project One of us A. Rana is thankful to the University Grant Commission, New Delhi, India for the award of Senior Research Fellowship.

Conflicts of Interest: The authors declare no conflict of interest.

References

- Jahnel, C. Heliatek Sets New Organic Photovoltaic World Record Efficiency of 13.2%-Heliatek—The Future Is Light. *Heliatek*, 8 February 2016; 2–3.
- Clarke, T.M.; Durrant, J.R. Charge Photogeneration in Organic Solar Cells. *Chem. Rev.* **2010**, *110*, 6736–6767. [CrossRef]

3. Cheng, Y.-J.; Yang, S.-H.; Hsu, C.-S. Synthesis of Conjugated Polymers for Organic Solar Cell Applications. *Chem. Rev.* **2009**, *109*, 5868–5923. [[CrossRef](#)]
4. Kurle, D.; Pflaum, J. Exciton Diffusion Length in the Organic Semiconductor Diindenoperylene. *Appl. Phys. Lett.* **2008**, *92*, 133306. [[CrossRef](#)]
5. Hammed, W.A.; Yahya, R.; Bola, A.L.; Mahmud, H.N.M.E. Recent Approaches to Controlling the Nanoscale Morphology of Polymer-Based Bulk-Heterojunction Solar Cells. *Energies* **2013**, *6*, 5847–5868. [[CrossRef](#)]
6. Dennler, G.; Mozer, A.J.; Juška, G.; Pivrikas, A.; Österbacka, R.; Fuchsbauer, A.; Sariciftci, N.S. Charge Carrier Mobility and Lifetime versus Composition of Conjugated Polymer/Fullerene Bulk-Heterojunction Solar Cells. *Org. Electron.* **2006**, *7*, 229–234. [[CrossRef](#)]
7. Deibe, C.; Strobe, T.; Dyakonov, V. Role of the Charge Transfer State in Organic Donor-Acceptor Solar Cells. *Adv. Mater.* **2010**, *22*, 4097–4111. [[CrossRef](#)]
8. Dimitrov, S.; Schroeder, B.; Nielsen, C.; Bronstein, H.; Fei, Z.; McCulloch, I.; Heeney, M.; Durrant, J. Singlet Exciton Lifetimes in Conjugated Polymer Films for Organic Solar Cells. *Polymers* **2016**, *8*, 14. [[CrossRef](#)]
9. Wilson, J.S.; Chawdhury, N.; Al-Mandhary, M.R.A.; Younus, M.; Khan, M.S.; Raithby, P.R.; Köhler, A.; Friend, R.H. The Energy Gap Law for Triplet States in Pt-Containing Conjugated Polymers and Monomers. *J. Am. Chem. Soc.* **2001**, *123*, 9412–9417. [[CrossRef](#)]
10. Rim, S.; Fink, R.F.; Schöneboom, J.C.; Erk, P.; Peumans, P. Effect of Molecular Packing on the Exciton Diffusion Length in Organic Solar Cells. *Appl. Phys. Lett.* **2007**, *91*, 173504. [[CrossRef](#)]
11. Singh, T.B.; Sariciftci, N.S.; Yang, H.; Yang, L.; Plochberger, B.; Sitter, H. Correlation of Crystalline and Structural Properties of C₆₀ Thin Films Grown at Various Temperature with Charge Carrier Mobility. *Appl. Phys. Lett.* **2007**, *90*, 213512. [[CrossRef](#)]
12. Bratsch, S.G. Revised Mulliken Electronegativities: II. Applications and Limitations. *J. Chem. Educ.* **1988**, *65*, 223. [[CrossRef](#)]
13. High-efficiency, S.; Coughlin, J.E.; Henson, Z.B.; Welch, G.C.; Bazan, G.C. Design and Synthesis of Molecular Donors for Solution-Processed High-Efficiency Organic Solar Cells. *Acc. Chem. Res.* **2014**, *47*, 257–270.
14. Chen, Y.; Wan, X.; Long, G. High Performance Photovoltaic Applications Using Solution-Processed Small Molecules. *Acc. Chem. Res.* **2013**, *46*, 2645–2655. [[CrossRef](#)]
15. Van Der Poll, T.S.; Love, J.A.; Nguyen, T.Q.; Bazan, G.C. Non-Basic High-Performance Molecules for Solution-Processed Organic Solar Cells. *Adv. Mater.* **2012**, *24*, 3646–3649. [[CrossRef](#)] [[PubMed](#)]
16. Blouin, N.; Michaud, A.; Gendron, D.; Wakim, S.; Blair, E.; Neagu-Plesu, R.; Belletête, M.; Durocher, G.; Tao, Y.; Leclerc, M. Toward a Rational Design of Poly(2,7-Carbazole) Derivatives for Solar Cells. *J. Am. Chem. Soc.* **2008**, *130*, 732–742. [[CrossRef](#)] [[PubMed](#)]
17. Henson, Z.B.; Zalar, P.; Chen, X.; Welch, G.C.; Nguyen, T.-Q.; Bazan, G.C. Towards Environmentally Friendly Processing of Molecular Semiconductors. *J. Mater. Chem. A Mater.* **2013**, *1*, 11117. [[CrossRef](#)]
18. Ernst, A.; Gobbi, L.; Vasella, A. Orthogonally Protected Dialkynes. *Tetrahedron Lett.* **1996**, *37*, 7959–7962. [[CrossRef](#)]
19. Tilley, J.W.; Zawiski, S. A Convenient Palladium-Catalyzed Coupling Approach to 2,5-Disubstituted Pyridines. *J. Org. Chem.* **1988**, *53*, 386–390. [[CrossRef](#)]
20. Handy, S.T.; Wilson, T.; Muth, A. Disubstituted Pyridines: The Double-Coupling Approach. *J. Org. Chem.* **2007**, *72*, 8496–8500. [[CrossRef](#)]
21. Wei, G.; Wang, S.; Renshaw, K.; Thompson, M.E.; Forrest, S.R. Solution-Processed Squaraine Bulk Heterojunction Photovoltaic Cells. *ACS Nano* **2010**, *4*, 1927–1934. [[CrossRef](#)]
22. Cai, S.; Chen, L.; Zha, D.; Chen, Y. A Novel Planar D-A Alternating Copolymer with D-A Integrated Structures Exhibiting H-Aggregate Behaviors for Polymer Solar Cells. *J. Polym. Sci. A Polym. Chem.* **2013**, *51*, 624–634. [[CrossRef](#)]
23. Bredas, J.-L.; Norton, J.E.; Cornil, J.; Coropceanu, V. Molecular Understanding of Organic Solar Cells: The Challenges. *Acc. Chem. Res.* **2009**, *42*, 1691–1699. [[CrossRef](#)] [[PubMed](#)]
24. Liu, B.; Chen, X.; Zou, Y.; Xiao, L.; Xu, X.; He, Y.; Li, L.; Li, Y. Benzo[1,2-B:4,5-B']Difuran-Based Donor-Acceptor Copolymers for Polymer Solar Cells. *Macromolecules* **2012**, *45*, 6898–6905. [[CrossRef](#)]
25. Liang, Y.; Xu, Z.; Xia, J.; Tsai, S.T.; Wu, Y.; Li, G.; Ray, C.; Yu, L. For the Bright Future-Bulk Heterojunction Polymer Solar Cells with Power Conversion Efficiency of 7.4%. *Adv. Mater.* **2010**, *22*, E125–E138. [[CrossRef](#)]
26. Liang, Y.; Feng, D.; Wu, Y.; Tsai, S.-T.; Li, G.; Ray, C.; Yu, L. Highly Efficient Solar Cell Polymers Developed via Fine-Tuning of Structural and Electronic Properties. *J. Am. Chem. Soc.* **2009**, *131*, 7792–7799. [[CrossRef](#)]
27. To, C.H.; Ng, A.; Dong, Q.; Djurišić, A.B.; Zapien, J.A.; Chan, W.K.; Surya, C. Effect of PTB7 Properties on the Performance of PTB7:PC₇₁ BM Solar Cells. *ACS Appl. Mater. Interfaces* **2015**, *7*, 13198–13207. [[CrossRef](#)]
28. Son, H.J.; Wang, W.; Xu, T.; Liang, Y.; Wu, Y.; Li, G.; Yu, L. Synthesis of Fluorinated Polythienothiophene-Co-Benzodithiophenes and Effect of Fluorination on the Photovoltaic Properties. *J. Am. Chem. Soc.* **2011**, *133*, 1885–1894. [[CrossRef](#)] [[PubMed](#)]
29. Liu, C.; Wang, K.; Gong, X.; Heeger, A.J. Correction: Low Bandgap Semiconducting Polymers for Polymeric Photovoltaics. *Chem. Soc. Rev.* **2016**, *45*, 4847. [[CrossRef](#)] [[PubMed](#)]
30. He, Z.; Xiao, B.; Liu, F.; Wu, H.; Yang, Y.; Xiao, S.; Wang, C.; Russell, T.P.; Cao, Y. Single-Junction Polymer Solar Cells with High Efficiency and Photovoltage. *Nat. Photonics* **2015**, *9*, 174–179. [[CrossRef](#)]
31. McKillop, A.; Turrell, A.G.; Young, D.W.; Taylor, E.C. Thallium in Organic Synthesis. 58. Regiospecific Intermolecular Oxidative Dehydromerization of Aromatic Compounds to Biaryls Using Thallium(III) Trifluoroacetate. *J. Am. Chem. Soc.* **1980**, *102*, 6504–6512. [[CrossRef](#)]

32. Aylward, J.B. Boron Trifluoride–Lead Tetra-Acetate: The Oxidation of Some Benzenoid Compounds. *J. Chem. Soc. B* **1967**, 1268–1270. [[CrossRef](#)]
33. Dou, L.; You, J.; Yang, J.; Chen, C.C.; He, Y.; Murase, S.; Moriarty, T.; Emery, K.; Li, G.; Yang, Y. Tandem Polymer Solar Cells Featuring a Spectrally Matched Low-Bandgap Polymer. *Nat. Photonics* **2012**, 6, 180–185. [[CrossRef](#)]
34. Sariciftci, N.S.; Smilowitz, L.; Heeger, A.J.; Wudi, F. Photoinduced Electron Transfer from a Conducting Polymer to Buckminsterfullerene. *Science* **1992**, 258, 1474–1476. [[CrossRef](#)] [[PubMed](#)]
35. Herath, N.; Das, S.; Keum, J.K.; Zhu, J.; Kumar, R.; Ivanov, I.N.; Sumpter, B.G.; Browning, J.F.; Xiao, K.; Gu, G.; et al. Peculiarity of Two Thermodynamically-Stable Morphologies and Their Impact on the Efficiency of Small Molecule Bulk Heterojunction Solar Cells. *Sci. Rep.* **2015**, 5, 13407. [[CrossRef](#)] [[PubMed](#)]
36. Wise, A.J.; Precit, M.R.; Papp, A.M.; Grey, J.K. Effect of Fullerene Intercalation on the Conformation and Packing of Poly-(2-Methoxy-5-(3'-7'-Dimethyloctyloxy)-1,4-Phenylenevinylene). *ACS Appl. Mater. Interfaces* **2011**, 3, 3011–3019. [[CrossRef](#)] [[PubMed](#)]
37. Jespersen, K.G.; Beenken, W.J.D.; Zaushitsyn, Y.; Yartsev, A.; Andersson, M.; Pullerits, T.; Sundström, V. The Electronic States of Polyfluorene Copolymers with Alternating Donor-Acceptor Units. *J. Chem. Phys.* **2004**, 121, 12613–12617. [[CrossRef](#)] [[PubMed](#)]
38. Sharenko, A.; Gehrig, D.; Laquai, F.; Nguyen, T.-Q. The Effect of Solvent Additive on the Charge Generation and Photovoltaic Performance of a Solution-Processed Small Molecule:Perylene Diimide Bulk Heterojunction Solar Cell. *Chem. Mater.* **2014**, 26, 4109–4118. [[CrossRef](#)]
39. Hwang, I.W.; Soci, C.; Moses, D.; Zhu, Z.; Waller, D.; Gaudiana, R.; Brabec, C.J.; Heeger, A.J. Ultrafast Electron Transfer and Decay Dynamics in a Small Band Gap Bulk Heterojunction Material. *Adv. Mater.* **2007**, 19, 2307–2312. [[CrossRef](#)]
40. Tong, M.; Coates, N.E.; Moses, D.; Heeger, A.J.; Beaupré, S.; Leclerc, M. Charge Carrier Photogeneration and Decay Dynamics in the Poly(2,7-Carbazole) Copolymer PCDTBT and in Bulk Heterojunction Composites with PC₇₀BM. *Phys. Rev. B* **2010**, 81, 125210. [[CrossRef](#)]
41. Keiderling, C.; Dimitrov, S.; Durrant, J.R. Exciton and Charge Generation in PC₆₀ BM Thin Films. *J. Phys. Chem. C* **2017**, 121, 14470–14475. [[CrossRef](#)]
42. Lee, C.H.; Yu, G.; Moses, D.; Srđanov, V.I.; Wei, X.; Vardeny, Z.V. Transient and Steady-State Photoconductivity of a Solid C₆₀ Film. *Phys. Rev. B* **1993**, 48, 8506–8509. [[CrossRef](#)] [[PubMed](#)]
43. Yamamoto, S.; Guo, J.; Ohkita, H.; Ito, S. Formation of Methanofullerene Cation in Bulk Heterojunction Polymer Solar Cells Studied by Transient Absorption Spectroscopy. *Adv. Funct. Mater.* **2008**, 18, 2555–2562. [[CrossRef](#)]
44. Bernardo, B.; Cheyns, D.; Verreet, B.; Schaller, R.D.; Rand, B.P.; Giebink, N.C. Delocalization and Dielectric Screening of Charge Transfer States in Organic Photovoltaic Cells. *Nat. Commun.* **2014**, 5, 3245. [[CrossRef](#)]
45. Rana, A.; Gupta, N.; Lochan, A.; Sharma, G.D.; Chand, S.; Kumar, M.; Singh, R.K. Charge Carrier Dynamics and Surface Plasmon Interaction in Gold Nanorod-Blended Organic Solar Cell. *J. Appl. Phys.* **2016**, 120, 063102. [[CrossRef](#)]

Disclaimer/Publisher’s Note: The statements, opinions and data contained in all publications are solely those of the individual author(s) and contributor(s) and not of MDPI and/or the editor(s). MDPI and/or the editor(s) disclaim responsibility for any injury to people or property resulting from any ideas, methods, instructions or products referred to in the content.